Bioengineered and Biocompatible Silver Nanoparticles From *Thalictrum Foliolosum* DC and Their Biomedical Applications

Sandip Kumar Chandraker
IGNTU: Indira Gandhi National Tribal University
Mishri Lal
IGNTU: Indira Gandhi National Tribal University
Preeti Dhruve
JNU: Jawaharlal Nehru University
Amit Kumar Yadav
IGNTU: Indira Gandhi National Tribal University
Rana P Singh
JNU: Jawaharlal Nehru University
Rajender S. Varma
Palacky University Olomouc: Univerzita Palackeho v Olomouci
Ravindra Sukla (ravindra.shukla@igntu.ac.in)
IGNTU: Indira Gandhi National Tribal University

Research Article

Keywords: Thalictrum foliolosum, Bioengineered, TF@AgNPs, Anticancer

Posted Date: January 24th, 2022

DOI: https://doi.org/10.21203/rs.3.rs-1273479/v1

Version of Record: A version of this preprint was published at Clean Technologies and Environmental Policy on May 9th, 2022. See the published version at https://doi.org/10.1007/s10098-022-02329-7.

Abstract

Bioengineered nanoparticles display unique characteristics at the cellular, atomic, and molecular levels with their geometric shapes dictating suitable actions and use. In the present study, bioengineered and bio-compatible silver nanoparticles (AgNPs) were obtained from *Thalictrum foliolosum* DC leaf extract (TFLE) which served as a capping and reducing agent. The effects of different parameters, such as varied concentrations of $AgNO_3$ (0.2, 0.5, 1.0, and 2.0 mM), TFLE (24.5, 24, 23.5, and 23 mL), pH (2, 4, 6, 7, and 8), and temperature (20, 40, 60, and 80 °C) were examined on the synthesis of *Thalictrum foliolosum*-assisted AgNPs (TF@AgNPs) and their characterization accomplished by UV-Vis and FTIR spectroscopy, XRD, TEM, SEM, and Zeta potential analyses. TEM and XRD results revealed that TF@AgNPs were spherical with ~18.27 ± 3.9 nm size. The biological studies indicate potential antifungal, antioxidant, and anticancer properties besides H_2O_2 sensing, for the ensued TF@AgNPs, suggesting their numerous biomedical appliances. A clean, cost-effective, and safer method for the procurement of bioengineered TF@AgNPs that precludes the use of any hazardous elements with no adverse effects are some additional sustainable attributes.

Introduction

Nanotechnology is a multidisciplinary and one of the most appealing research areas, as the use of nanoparticles (NPs) in various fields has increased extensively in recent years (Schröfel et al. 2014; Sharma et al. 2021; Singh et al. 2021). One-dimensional, small sized (1-100 nm) NPs have a high surface to volume ratio and are highly reactive. The effect of this specific property of NPs, different from their bulk materials, has been observed in diverse disciplines, including chemical (Varma 2019), biomedical (Iravani and Varma 2020), agricultural (Nasrollahzadeh et al. 2020) and engineering (Lu et al. 2021) research. AgNPs have garnered consideration in current decade because of their broad spectrum of applications in the areas of the environment, sensing, catalysis, optics, electronics, nanomedicine, biomedical devices, and antimicrobial applications due to their unusual intrinsic physiochemical and vigorous antibacterial activities (Sharma et al. 2021).

Among the two approaches, top-down, and bottom-up, latter entails the assembly of single atoms or molecules to create NPs (Polshettiwar et al. 2009) often via physical, chemical, and biological methods; biogenic approach, in contrast to physical and chemical methods, precludes the use and generation of hazardous materials (Zare et al. 2020). The ecofriendly greener synthesis of AgNPs has been accomplished using plant extracts, microorganism, antioxidants, biosurfactants, and enzymes used as reducing and capping/stabilizing agents (Hebbalalu et al. 2013) which are economical and biocompatible processes (Moulton et al. 2010) and are ideal for large-scale processing.

Fungal diseases are severe health problem worldwide and effective therapies and management strategies must be increased (Scorzoni et al. 2017) via the production of low-cost and less toxic new antifungal drugs (Bocate et al. 2019). It has been reported that berberine present in the leaves of *T. foliolosum* has antioxidant and antifungal activity (Kumar et al. 2020). In this context, the synergistic

effect of NPs and active ingredients would provide better results than drugs alone as affirmed by some previous findings (Kaur et al. 2019; Bankier et al. 2019; Mohsen et al. 2020).

Hydrogen peroxide (H_2O_2) has been widely used green oxidant applied in various fields such as pharmacology, wood, food, textiles, electronics, wastewater treatment, cosmetics, tanning, and pulp industries (Li et al. 2019; Chandraker et al. 2019; Chandraker et al. 2021a); global demand for the H_2O_2 market being 3,850 kilotons in 2015 is expected to reach ~ 6,000 kilotons by 2024 (Shi et al. 2017; Kim et al. 2018). However, the accumulation and even a minimal volume of H_2O_2 in the process can lead to numerous safety and environmental hazards due to its toxicity (Tagad et al. 2013). Therefore, accurate, stable, and expeditious methods for detecting H_2O_2 residues in commercially available goods are necessary among available means for sensitive detection of H_2O_2, namely spectrometric method, chemiluminescence, optical detection, electrochemical and batch-injection analysis (Silva et al. 2012; Hsu et al. 2015). There is potential scope to detect H_2O_2 using bioengineered AgNPs as has been suggested by the limited available studies (Rani et al. 2020).

The global burden of cancer is on the rise, and chemotherapeutics are one of the most widely methods for the treatment of cancer. GLOBOCAN report from 2018, revealed 18.1 million cancer cases, with death toll of 9.6 million (Bray et al. 2018). The advancement in nanomedicine provides a ray of hope and has made it an attractive option for cancer therapeutics because of its multifunctionality (Aghebati-Maleki et al. 2020), as the nano-based systems are being studied for various appliances, ranging from drug delivery to overcome drug resistance to imaging (Iravani and Varma 2021). The presence of cytotoxic alkaloids present in the leaves of *Thalictrum foliolosum* DC indicates that the AgNPs generated from them might be potent against cancer cells.

Thalictrum foliolosum DC. (Fig. 1) is a worldwide distributed tall perennial medicinal plant with ~ 200 species belonging to the family: Ranunculaceae with several diverse uses (Sun and Han 2019). The present study was therefore undertaken to bioengineer, optimize, and characterize silver nanoparticles (AgNPs) from *T. foliolosum* leaf extract (TFLE) and evaluate their antifungal, H_2O_2 sensing, antioxidant, and anticancer properties.

Materials And Methods

Collection of plant material

Fresh leaves of *T. foliolosum* were obtained from Kapildhara site of Amarkantak, MP, India in January 2019, duly authenticated by a taxonomist and a herbarium specimen (DoB/10/ TF/98-2019) was submitted to the Department of Botany, IGNTU, Amarkantak (India).

Chemicals

Himedia (Mumbai, India) provided silver nitrate ($AgNO_3$), H_2O_2, and potato dextrose agar (PD-A), potato dextrose broth (PD-B), 2,2-diphenyl-1-picrylhydrazyl (DPPH), and 2,2-azino-bis-3-ethylbenzothiazoline-6-

sulphonic acid (ABTS). All the chemicals used were of AR grade. All the equipment was cleaned with double distilled water (DDW) and placed in an oven (Scientech).

Formulation of plant extract

The deionized water was used to wash the leaves of *T. foliolosum*. About 20 grams of the leaves were weighed and cut into identical pieces. Sliced leaves were placed in a 750 mL borosilicate flask with deionized water (200 mL), and boiled for 25 minutes at 65 ^{0}C. The filtrate (TFLE) was collected using Whatman No. 1 filter paper, and kept at 4 ^{0}C.

Phytochemical investigation

The main phyto-constituents of TFLE were identified with the slight modification of the following earlier described protocol Chandraker et al. (2020), the main components being starch, lipid, protein, tannins, alkaloids, saponins, glucosides, mucilage, cellulose, and pectin.

Optimization of TF@AgNPs

Different reaction parameters like TFLE and $AgNO_3$ concentration, pH, and temperature were optimized to obtain the maximum and stable synthesis of TF@AgNPs. To optimize the temperature, 1 mL TFLE was blended with 24 mL $AgNO_3$ (0.1 mM) and incubated at 20, 40, 60, and 80 ^{0}C for 80 min. The same experiment was then repeated at varying pH's (2, 4, 7, 6, and 8) and incubated at 28 ^{0}C for 80 minutes to optimize the pH. One mM $AgNO_3$ (0.5, 1.5, and 2.0 mL) solutions were mixed with varying amounts of TFLE (24.5, 24, 23.5, and 23 mL) and incubated at 28 ^{0}C for 80 minutes to optimize TFLE concentration. To optimize $AgNO_3$ concentration, 1 mL of different $AgNO_3$ concentrations (0.2, 0.5, 1.0, and 2.0 mM) were added to 24 mL of TFLE and incubated at 28 ^{0}C for 80 minutes. The sample was analyzed deploying UV–visible absorption spectroscopy to confirm the optimum formation of TF@AgNPs.

Physicochemical characterization of TF@AgNPs

UV-visible spectroscopy (Shimadzu UV-1800) was performed to confirm the phytosynthesis of TF@AgNPs. To affirm the crystallinity of TF@AgNPs, XRD analysis was carried out applying Bruker D8 X-Ray Diffractometer at 30 kV and 20 mA current with Cu K (I = 1.54 A). FTIR (Bruker, Germany. Model: Vertex 70) spectral studied were done with Potassium bromide at 0.5 cm^{-1} resolution. In order to determine the size and shape of NPs, ultramicroscopic images were obtained using a transmission electron microscope (Technai G20 FEI) operating with 200 kV, and a current of 104 beam. An scanning electron microscope (EVO 18; Carl Zeiss, Germany) attached to energy dispersive X-ray (EDS/EDAX) was used to study the elemental configuration and morphology of TF@AgNPs. The average size of the particles, the size distribution, and zeta potential were calculated (Anton Paar, Litesizer 500).

Applications of TF@AgNPs

Antifungal activity

The aflatoxin producing and post-harvest food spoiling fungi *Aspergillus flavus* (MTCC No. 277) was selected to evaluate the fungitoxic potential of TF@AgNPs. *A. flavus* was secured from the Microbial Type Culture Collection and Gene Bank (MTCC) of the Institute of Microbial Technology (IMTECH), Chandigarh, India. The anti-proliferative test for the mycelia inhibition of treated fungi was performed using semi-solid PDA media, combined with varying concentrations of TF@AgNPs (1.25, 2.5, 5.0, 10.0, and 20.0 mg/20 mL). Finally, a spore suspensions of 1×10^6CFU mL^{-1} was inoculated in a 2 mm well at the center of each plate. Similar plates except TF@AgNPs were kept as negative controls, whereas TFLE and $AgNO_3$ solutions were tested in different plates as positive controls. The test was performed in triplicate and all the petri dishes were kept at 30 ^{0}C for six days in a BOD incubator. The radial growth of the fungal colony was measured and the photographs were captured thereafter. Percent fungal inhibition was ascertained following percent inhibition of radial growth (IRG) as follows:

$$IRG\ (\%) = \left[\frac{R_1 - R_2}{R_1}\right] \times 100$$

Where R_1 is radial growth in control's, and R_2 stands for radial growth in various treatments. Data were analyzed with mean ± SE.

H_2O_2 sensing activity

To detect the H_2O_2 sensing capability of TF@AgNPs, the colloidal solution of TF@AgNPs (3 mL) was carefully mixed with 20 mM H_2O_2 (1 mL). Before adding H_2O_2, the initial absorption spectrum of TF@AgNPs solution was recorded at 450 nm. UV-Vis spectroscope (Shimadzu UV-1800) was used to record the deviation in the characteristic peak after a periodic spell of 3 minutes.

Antioxidant activity

The antioxidant activity of TF@AgNPs was assessed using the DPPH and ABTS free radical inhibition tests, as described by Chandraker et al. (2019). The reduction of stable free radicals DPPH and ABTS by TF@AgNPs was determined following UV-visible spectroscopy, and the results were compared with reference antioxidant ascorbic acid. The percentage scavenging activity was calculated using the following formula:

$$\%\ scavenging\ activity\ = \left[\frac{Absorbance\ of\ control - Absorbance\ of\ sample}{Absorbance\ of\ control}\right] \times 100$$

Anticancer activity

Cancer cell lines A431 and B16F10 were cultured and stored at 38° C with 5% carbon dioxide in Dulbecco's Modified Eagle's (DME) medium containing 10% FBS and 1% penicillin-streptomycin-amphotericin B cocktail. The modified standard MTT assay of Singh et al. (2013) was used to determine the anticancer efficacy of TF@AgNPs against A431 (squamous cell carcinoma cell line) and B16F10

(melanoma cell line). Nanoparticles for treatment were dispersed in DMSO with the final concentration of DMSO was 0.1% in the medium. In a 96-well plate, both types of cells were seeded at a density of 5000 cells per well. After 24 hours of seeding, cells were treated for 24 and 48 hours with varying concentrations of TF@AgNPs (10, 25, 50, and 100 g/ml), after which the medium was gently switched with the MTT solution and incubated for four hours at 37°C. To dissolve the ensued formazan crystals, 100 µL of DMSO was added, and the plates were further kept for 10 min at 37°C. The absorbance was measured at 570 nm using a microplate reader.

The percentage cell viability was calculated with following formula:

$$\%\ cell\ viability = \left[\frac{Aaverage\ absorbance\ of\ the\ treated\ sample}{Average\ absorbance\ of\ the\ control\ sample}\right] \times 100$$

Statistical analysis

All of the experiments were repeated for three times, and the results were calculated in mean ± SE using OriginPro 8.5 software. Data from the MTT assay were examined using the Student's t-test, with $P < 0.05$ considered statistically significant.

Results And Discussion

In this study, bioengineered TF@AgNPs were obtained aqueous TFLE as a reducing and capping agent, and their antifungal, H_2O_2, antioxidant, and anticancer properties were evaluated.

Phytochemical analysis

T. foliolosum is a well-known plant for its phytochemicals with an abundance of alkaloids (Bhakuni and Singh 1982). According to Ringmichon et al. the rhizomes of *T. foliolosum* contain starch, lipid, protein, tannins, alkaloids, saponins, glucosides, mucilage, cellulose, and pectin (Ringmichon et al. 2013). In our study, these phytochemicals in the THLE were confirmed (Table 1) which can be coated on the surface of Ag^+ and thus liable for the reduction of Ag^+ to (Ag^0) and further preventing their agglomeration as corroborated by deployment of alkaloids (Almadiy and Nenaah 2018), tannins (Lakshmanan et al. 2018), and saponins (Choi et al. 2018).

Table 1
Phytochemical analysis of TFLE.

S. No.	Phytochemicals	Test	Result
1.	Alkaloids	Mayer's test, Wagner test	**+ve**
		Dragendroff test	**+ve**
2.	Flavanoids	Ferric chloride test and Lead acetate test	**+ve**
3.	Diterpenes	Copper acetate test	**-ve**
4.	Tannins	Ferric chloride test	**+ve**
5.	Glycosides	Molish test	**-ve**
6.	Saponins	Foam test	**-ve**
7.	Triterpenes	Salkowski test, Liberman test	**-ve**
8.	Phlobatannins	HCL test	**+ve**
9.	Steroids	Salkowski test	**-ve**
10.	Cardiac glycoside	Keller kilanis test	**-ve**
+ve, Present; and -ve, Absent			

Synthesis of TF@AgNPs and their optimization

The addition of TFLE to the aqueous solution of 2 mM silver nitrate resulted in a color change from colorless to dark brown solution, as shown in the inset of Fig. 2. After 80 min at room temperature (28 ^{0}C) of reaction time, a signature surface plasmon resonance (SPR) band with λmax emerged at 450 nm. At the same time, no absorption spectra were observed in aqueous TFLE and $AgNO_3$ solution. Optimization studies were performed to improve the yield of TF@AgNPs. Several experiments with different parameters, such as reaction times, the concentration of TFLE and silver nitrate, temperature, and optimal pH, were used to achieve a narrow size distribution of TF@AgNPs.

Effect of reaction time

Figure 2, shows UV-vis spectra of bioengineered TF@AgNPs while their formation was monitored every 10 min. time intervals. Maximum reduction and formation of AgNPs was observed and no impact on absorption spectra after 80 min. of reaction of $AgNO_3$ and TFLE. Even after one month, the TF@AgNPs showed an absorption peak of 450 nm thus affirming their stability.

Effect of temperature

To evaluate the influence of temperature on TF@AgNPs synthesis, TFLE (1 mL) was mixed with 2 mM $AgNO_3$ (9 mL) in four different vials and incubated at varying temperatures from 20 to 80°C. After this optimization study, it became clear that raising the temperature of the reaction mixture increases the synthesis of bioengineered NPs; the maximum synthesis of AgNPs was observed at 80°C Fig. 3(a). There was a positive impact of temperature on the reaction mixture because high temperature increased the kinetic energy of molecules present in the solution and led to a faster synthesis rate (Saxena et al. 2016).

Effect of pH

During the synthesis of NPs, the reaction mixture's pH plays a significant role; even the color of the reaction mixture, the intensity of the SPR peaks, shape, and size of the nanoparticles were pH dependent. In our study, the acidic pH 2 and pH 4 shows a low absorption peak at 450 nm compared to pH 6 and 8. Therefore, the alkaline pH 8 was optimal for the synthesis of NPs Fig. 3(b). According to Vanaja et al. (2013) the absorption increased when pH increased, indicating that the alkaline medium gave better results than the acidic medium for NPs synthesis.

Effect of TFLE concentration

Another vital factor for the greener synthesis of NPs is the concentration of leaf extract. The UV–vis absorption spectra of TF@AgNPs were prepared using varying concentrations of TFLE (0.5, 1, 1.5, and 2 mL), where the $AgNO_3$ concentration was kept constant at 2 mM. Fig. 3(c) depicts that in 0.5 TFLE concentrations, there is no SPR peak. After increasing the concentration of TFLE, SPR peaks were proportionally enhanced, the maximum peak intensity being observed at a TFLE dose of 2.0 mL. The synthesis of bioengineered NPs was enhanced by the increased concentration of biomolecules involved in metal reduction as has been reported earlier for the *Pongamia pinnata* leaf extract (Priya et al. 2016) and the *Citrullus lanatus* fruit rind extracts (Ndikau et al. 2017).

Effect of $AgNO_3$ concentration

In order to find impact of substrate on NPs synthesis, different concentrations of $AgNO_3$ solution (0.2, 0.5, 1, and 2 mM) were used to synthesize TF@AgNPs and their formation were monitored by UV–Vis spectral analysis thus evidencing the correlation between concentrations of $AgNO_3$ solution and TF@AgNPs during the synthesis. In our study, the absorption peak for TF@AgNPs was found to be low at lower concentrations viz. 0.5 and 1.0 mM (Fig. 3d), presumably due to very less availability of Ag^+ in the reacting solution. The UV- vis spectrophotometer displayed significant absorption spectra at 450 nm with 1.0 and 2.0 mM $AgNO_3$. Therefore, 2 mM $AgNO_3$ solution is thought to be the optimum concentration for the phytosynthesis of AgNPs.

Characterization of TF@AgNPs

XRD analysis

The X-ray diffraction was performed to confirm that the TF@AgNP formed were crystalline in nature (Fig. 4). The TF@AgNP metal formed in our study show the form of fcc crystalline lattice as evidenced by the peaks at 2θ = 38.24, 44.33, 64.49, and 77.49 which were clearly representing the (111), (200), (220), and (311) Bragg's reflections of the face-centered cubic structure of silver. A comparison of the XRD data with the standard data confirmed it's crystalline in nature, and these planes correspond to the standard JCPDS file no. 04-0783 (Pattanayak et al. 2017).

FT-IR spectral analysis

FT-IR analysis was performed for the detection of functional groups which are present in the THLE and the surface of Ag^0. The wave number and interpretation of probable functional groups of TF@AgNPs, and leaf extract of *T. foliolosum* are shown in Table 1 in SI.

TEM, SEM and EDX analysis

TEM images of TF@AgNPs are shown in Fig. 5(a) and (b), which reveals the formation of isotropic spherical AgNPs, the average particle size being 18.27 ± 3.9 nm. This corresponds to the particle size spectrum calculated from the UV-Vis spectroscopy SPR band, and XRD.

SEM analysis revealed the shape and structure of TF@AgNPs, confirming the formation of homogeneous TF@AgNPs (Fig. 5c and d). The composition of the elements in TF@AgNPs was revealed using energy-dispersive X-rays (EDX). At 3 keV, the EDX displayed the major elemental peak, indicating metallic silver in Figure 6 (a). After the quantitative estimation, elemental Ag was recorded with the highest weight percentage i.e. 84.17%, whereas, O, Si, S, Cl, and Ca have 10.00, 0.63, 0.03, 4.74, and 0.43% respectively (Fig. 6).

Zeta particle size and potential

DLS measurements were carried out to actuate the size, distribution of particle, and zeta potential of TF@AgNPs in aqueous phase. Zeta particle size was employed to determine the average size of TF@AgNPs, while zeta potential reveals the stability of bioengineered NPs in the aqueous medium. Fig. 1(a) in the supplementary material shows that the corresponding average zeta particle size is 65.11 nm and polydispersity index (PDI) of 25.4. Because DLS measurements were based on the hydrodynamic radius of the particles in the aqueous medium, the particle size distribution was found higher than the average particle size of TEM. Fig. 1(b) in the supplementary material shows that the corresponding zeta potential of TF@AgNPs is -21.0 mV, suggesting the stability of AgNPs. The capping of phytoconstituents, which are present in the TFLE, could explain the substantial negative potential value.

Applications of TF@AgNPs

Antifungal activity of TF@AgNPs

Aspergillus sp. are ubiquitous fungi mainly found in stored grains. Certain *Aspergillus* species produce toxins that can harm human and animal health and lead to hepatic, nephrotoxicity, immunosuppression,

and carcinogenicity (Bocate et al. 2019). Following an incubation period of 6 days, the inhibitory effect of different concentrations of TF@AgNPs against *Aspergillus flavus* is shown in Fig. 7. In our study, we observed that the mycelial growth of *A. flavus* is directly depended on the concentration of TF@AgNPs. Inhibition of radial growth (IRG) was increased when concentration of TF@AgNPs increased (Fig. 7). Bocate et al. described the effect of AgNPs in different *Aspergillus* species while Pariona et al. observed similar results for copper nanoparticles against different fungal species (Bocate et al. 2019; Pariona et al. 2019). As compared to control, treated plates of *A. flavus* show lighter color, reduced colony, and texture. Fig. 8, depicts a bar graph showing IRG of TF@AgNPs against the *A. flavus*. At higher concentrations of 20 mg/20 mL, NPs showed highest (84.48%) IRG and at 1.25 mg/ 20 mL, IRG was 37.17. Besides, the IRG was found to be 21.59, 11.26, 42.71, 48.42, and 55.39% against TFLE, $AgNO_3$, and 2.5, 5, and 10 mg/20 mL concentrations of NPs, respectively.

Our outcomes are important because the second major cause of invasive aspergilloses after *Aspergillus fumigatus* is *A. flavus*, and superficial infection is the most common cause of it (Hedayati et al. 2007). It can be concluded that bioengineered TF@AgNPs exerts substantial *in-vitro* antifungal activity against *A. flavus* which could be attributed to sufficient particle size and the capping and reducing agent used in the synthesis process, which originates from TFLE. In a similar investigation, Jaffri and Ahmad confirmed antifungal activity of *Prunus cerasifera* fruit extract mediated AgNPs against *A. flavus* (Jaffri et al. 2018).

H_2O_2 sensing properties

The precise detection and quantitative analysis of H_2O_2 is an essential requirement in the processes of food sterilization, the production of pharmaceuticals, and medical devices (Neal et al. 2017). Therefore, it is imperative to design a consistent and efficient technique for detecting the H_2O_2. In our study, the bioengineered TF@AgNPs were assessed with potential H_2O_2 sensing capacity. Using the UV-visible spectrophotometer, the initial SPR spectrum of diluted TF@AgNPs solution (3 mL) was recorded. In the TF@AgNPs solution 1 mL of 20 mM H_2O_2 was applied, and relative spectra were observed at frequent intervals as shown in the Fig. 9. After the reaction with H_2O_2 dark brown color of TF@AgNPs Fig. 9 (vial i) gradually disappeared as shown in (vial iii) and finally became colorless after 21 min shown in the Fig. 9 (vial iii). There were no changes in the color of control set without H_2O_2 and SPR absorbance remains the same. The H_2O_2 sensing properties efficiency of TF@AgNPs is further compared with previously published AgNPs Table 2 in the supplementary material.

aratale et al., have suggested that the generation of free radicals due to the reaction of AgNPs with H_2O_2 is responsible for the degradation of AgNPs (Saratale et al. 2019). The probable catalytic reaction of sensing H_2O_2 depends on the redox reaction. An electron shifted from the surface of reduced site TFLE capped TF@AgNPs to H_2O_2 producing an OH• radical, and one more electron shifted from H_2O_2 to an oxidized surface of the TF@AgNPs to generate HO_2• radical. Finally, when the H_2O• radical reacts with OH• radical, H_2O) and O_2 are generated (Aadil et al. 2016). The following redox reaction mechanism summarizes the probable H_2O_2 decomposition reaction process by TF@AgNPs.

$$H_2O_2 + Ag^0 \rightleftharpoons Ag^+ + OH^* + OH^-$$

$$OH^- + H_2O_2 \rightleftharpoons HO_2^- + H_2O$$

$$HO_2^- + Ag^+ \rightleftharpoons HO_2^* + Ag^0$$

$$HO_2^* + OH^* \rightleftharpoons H_2O + O_2$$

Antioxidant capability

The results of the DPPH and ABTS radical scavenging experiments, both of which are relatively quick and sensitive, confirmed the antioxidant potential of TF@AgNPs. DPPH is a well known stable free radical having maximum UV-Vis absorption within the range of 515-520 nm. This organic nitrogen radical having purplish-blue color, and converts into a colorless or pale-yellow when it reacts with substance with hydrogen/electron donor and its absorbance decreases (Khorrami et al. 2019; Chandraker et al. 2021b). The frequency of the transition of color depends on the concentration and nature of the sample. Antioxidant capability of TF@AgNPs was dose dependent as shown in Fig. 10(a) and (b). The DPPH radical inhibition of TF@AgNPs for the concentration range of 31.25 to 500 μgmL^{-1} was found to be around 85.05 ± 0.04 to 92.74± 0.02% with 75.20 μgmL^{-1} IC_{50} Fig. 10(a). For the standard compound ascorbic acid in the same concentration range free radical inhibition was observed from 75.64 ± 0.08 to 98.94 ± 0.03% with 41.5 μgmL^{-1} IC50. Salari et al. (2019), and Vorobyova et al. (2020) reported similar DPPH free radical scavenging activities from *Prosopis farcta* fruit extract and black currant pomace extract AgNPs. Similarly, at 31.25 to 500 mg mL^{-1} concentrations of TF@AgNPs ABTS radical inhibition was found to be 15.67 ± 0.30 to 80.67 ± 0.05% with 168.62 μgmL^{-1} IC_{50}. However, at the same concentration, ascorbic acid showed 38.39 ± 0.05 to 88.09 ± 0.1% inhibition with 173.12 μgmL^{-1} IC_{50}. Fig. 10(b).

Anticancer activity

In vitro anticancer activity of TF@AgNPs against cancer cell lines, A431 and B16F10 was determined by MTT assay. It is a colorimetric assay that detects cell viability by reducing the yellow colour dye 3-(4,5-dimethylthiazol-2-yl)-2,5-diphenyl tetrazolium bromide (MTT) with the mitochondrial enzyme succinate dehydrogenase to generate formazan crystals. The cell viability of both A431 and B16F10 cells was shown to be reduced after 24 and 48 hours of treatment; and the viability of cancer cells was reduced in a concentration-dependent manner. TF@AgNPs at the concentration of 100 µg/ml caused ~20% and ~50% decrease in the survival of A431 and B16F10 cells, respectively, compared to control (Fig. 11). The decrease in cell viability was profound in case of B16F10 cells where significant decrease ($P<0.05$) in the cell viability was observed. After 24 hours of treatment, TF@AgNPs was shown to be more effective against B16F10 cell lines with an IC50 of 98.89 µg/mL compared to A431 cell lines with an IC50 of 231.37 µg/mL. AgNPs are known to produce reactive oxygen species (ROS), which can contribute to

oxidative damage., and there are reports about induction of apoptosis through caspase 9/3 dependent pathway by AgNPs through ROS generation under *in vitro* conditions (Ahamed et al. 2010). The cytotoxic effect of AgNPs could also be due to the inorganic nanoparticles being taken up by the cell and their enhanced interaction with DNA and proteins, however for the detailed mechanisms further studies are needed (Franskevych et al. 2016). Additionally, alkaloids have also been isolated from *T. foliolosum* having cytotoxic activity against malignant cancer cell lines such as A549, BGC823, Hep-G2, HL60, MCF7, and SW480 (Sun et al. 2019). Thus the secondary metabolites might also be contributing towards the enhanced cytotoxicity of TF@AgNPs.

Conclusions

We have bioengineered AgNPs by deploying pharmacologically active *Thalictrum foliolosum* DC leaf extract as a cost-effective and eco-friendly strategy. The ensued TF@AgNPs were characterized by using standard techniques namely UV-Vis, XRD, FTIR, TEM, SEM, EDX spectroscopy, and zeta size and potential. The antifungal activity of TF@AgNPs was scrutinized against *A. flavus* where they showed the highest antifungal activity at higher concentration 20 mg/20 mL. Cytotoxic activity of TF@AgNP was established against skin cancer cell lines A431 and B16F10, with higher efficiency towards B16F10 cells. The capability of TF@AgNPs to detect hydrogen peroxide renders them suitable agents for nano-remediation of pollutants and ROS. To our knowledge, this is the first investigation on the biological properties of *Thalictrum foliolosum* DC leaf extract-mediated AgNPs, which bodes well for their prospective application in biomedical sciences. Similarly, the findings revealed here lay the groundwork for future applications of AgNPs in cancer treatment. The diverse and relevant outcomes of the synthesised TF@AgNPs and their generation via a cost-effective and eco-friendly method holds promise in future biological studies with appropriate change in the size and form of the metallic NPs.

Declarations

Conflict of Interest

Authors declare no conflict of interest.

Author Contributions

All authors listed have made a substantial, direct and intellectual contribution to the work, and approved it for publication

Acknowledgments

The authors are thankful to the Science and Engineering Research Board (SERB), Department of Science and Technology, New Delhi for financial assistance (YSS/2015/002080). Authors gratefully acknowledge the necessary instrumental facilities of UGC-DAE Consortium for Scientific Research, Indore, and Sophisticated Analytical Instrumentation Facility, AIIMS, New Delhi. Authors are thankful to the

department of pharmacy for providing Zeta particles size and potential facility, IGNTU, Amarkantak, MP, India.

References

1. Aadil KR, Barapatre A, Meena AS, Jha H (2016) Hydrogen peroxide sensing and cytotoxicity activity of Acacia lignin stabilized silver nanoparticles. Int J Biol Macromol 82:39-47. https://doi.org/10.1016/j.ijbiomac.2015.09.072
2. Aghebati-Maleki A, Dolati S, Ahmadi M, Baghbanzhadeh A, Asadi M, Fotouhi A, Yousefi M, Aghebati-Maleki L (2020) Nanoparticles and cancer therapy: Perspectives for application of nanoparticles in treatment of cancers. J Cell Physiol 235(3):1962-72. https://doi.org/10.1002/jcp.29126
3. Ahamed M, Posgai R, Gorey TJ, Nielsen M, Hussain SM, Rowe JJ (2010) Silver nanoparticles induced heat shock protein 70, oxidative stress and apoptosis in Drosophila melanogaster. Toxicol Appl Pharmacol 242(3):263-69. https://doi.org/10.1016/j.taap.2009.10.016
4. Almadiy AA, Nenaah GE (2018) Ecofriendly synthesis of silver nanoparticles using potato steroidal alkaloids and their activity against phytopathogenic fungi. Braz Arch Biol Technol 61. https://doi.org/10.1590/1678-4324-2018180013
5. Bankier C, Matharu RK, Cheong YK, Ren GG, Cloutman-Green E, Ciric L (2019) Synergistic antibacterial effects of metallic nanoparticle combinations. Sci Rep 9(1):16074. https://doi.org/10.1038/s41598-019-52473-2
6. Bhakuni DS, Singh RS (1982) The alkaloids of *Thalictrum foliolosum*. J Nat Prod 45(3):252-55. https://doi.org/10.1021/np50021a003
7. Bocate KP, Reis GF, de Souza PC, Junior AGO, Durán N, Nakazato G, Furlaneto MC, de Almeida RS, Panagio, LA (2019) Antifungal activity of silver nanoparticles and simvastatin against toxigenic species of Aspergillus. Int J Food Microbiol 291:79-86. https://doi.org/10.1016/j.ijfoodmicro.2018.11.012
8. Bray F, Ferlay J, Soerjomataram I, Siegel RL, Torre LA, Jemal A (2018) Global cancer statistics 2018: GLOBOCAN estimates of incidence and mortality worldwide for 36 cancers in 185 countries. CA: a cancer journal for clinicians, 68(6):394-24. https://doi.org/10.3322/caac.21492
9. Chandraker SK, Lal M, Dhruve P, Singh RP, Shukla R (2021a) Cytotoxic, antimitotic, DNA binding, photocatalytic, H_2O_2 sensing, and antioxidant properties of biofabricated silver nanoparticles using leaf extract of *Bryophyllum pinnatum* (Lam.) Oken. Front Mol Biosci 2021:465. https://doi.org/10.3389/fmolb.2020.593040
10. Chandraker SK, Lal M, Ghosh MK, Tiwari V, Ghorai TK, Shukla R (2020) Green synthesis of copper nanoparticles using leaf extract of *Ageratum houstonianum* Mill. and study of their photocatalytic and antibacterial activities. Nano Express 1(1). https://doi.org/10.1088/2632-959X/ab8e99.
11. Chandraker SK, Lal M, Kumar A, Shukla R (2021b) *Justicia adhatoda* L. mediated green synthesis of silver nanoparticles and assessment of their antioxidant, hydrogen peroxide sensing and optical

properties. Mater Technol 10:1-1. https://doi.org/10.1080/10667857.2021.1949525

12. Chandraker SK, Lal M, Shukla R (2019) DNA-binding, antioxidant, H_2O_2 sensing and photocatalytic properties of biogenic silver nanoparticles using *Ageratum conyzoides* L. leaf extract. RSC Adv 9(41):23408-17. https://doi.org/10.1039/C9RA03590G
13. Choi Y, Kang S, Cha SH, Kim HS, Song K, Lee YJ, Kim K, Kim YS, Cho S, Park Y (2018) Platycodon saponins from *Platycodi radix* (*Platycodon grandiflorum*) for the green synthesis of gold and silver nanoparticles. Nanoscale Res Lett 13(20):1-10. https://doi.org/10.1186/s11671-018-2436-2
14. Franskevych DV, Grynyuk II, Prylutska SV, Matyshevska OP (2016) Modulation of cisplatin-induced reactive oxygen species production by fullerene C60 in normal and transformed lymphoid cells. Ukr Biochem J 88(1):44-50. http://dx.doi.org/10.15407/ubj88.01.044
15. Hebbalalu D, Lalley J, Nadagouda MN, Varma RS (2013) Greener techniques for the synthesis of silver nanoparticles using plant extracts, enzymes, bacteria, biodegradable polymers, and microwaves. ACS Sustainable Chem Eng 1(7):703-12. https://doi.org/10.1021/sc4000362
16. Hedayati MT, Pasqualotto AC, Warn PA, Bowyer P, Denning DW (2007) *Aspergillus flavus*: human pathogen, allergen and mycotoxin producer. Microbiol 153(6):1677-92. DOI 10.1099/mic.0.2007/007641-0
17. Hsu CC, Lo YR, Lin YC, Shi YC, Li PL (2015) A spectrometric method for hydrogen peroxide concentration measurement with a reusable and cost-efficient sensor. Sens 15(10):25716-29. https://doi.org/10.3390/s151025716
18. Iravani S, Varma RS (2020) Sustainable synthesis of cobalt and cobalt oxide nanoparticles and their catalytic and biomedical applications. Green Chem 22(9):2643-61. https://doi.org/10.1039/D0GC00885K
19. Iravani S, Varma RS (2021) MXenes for Cancer Therapy and Diagnosis: Recent Advances and Current Challenges. ACS Biomater Sci Eng 7:1900–13. https://doi.org/10.1021/acsbiomaterials.0c01763
20. Jaffri SB, Ahmad KS (2018) Augmented photocatalytic, antibacterial and antifungal activity of pruno synthetic silver nanoparticles. Artif. Cells Nanomed Biotechnol 46(1):127-37. https://doi.org/10.1080/21691401.2017.1414826
21. Kaur A, Preet S, Kumar V, Kumar R, Kumar R (2019) Synergetic effect of vancomycin loaded silver nanoparticles for enhanced antibacterial activity. Colloids Surf B 176:62-69. https://doi.org/10.1016/j.colsurfb.2018.12.043
22. Khorrami S, Zarepour A, Zarrabi A (2019) Green synthesis of silver nanoparticles at low temperature in a fast pace with unique DPPH radical scavenging and selective cytotoxicity against MCF-7 and BT-20 tumor cell lines. Biotechnol Rep 24:p.e00393. https://doi.org/10.1016/j.btre.2019.e00393
23. Kim HW, Ross MB, Kornienko N, Zhang L, Guo J, Yang P, McCloskey BD (2018) Efficient hydrogen peroxide generation using reduced graphene oxide-based oxygen reduction electrocatalysts. Nat Catal 1(4):282-90. https://doi.org/10.1038/s41929-018-0044-2

24. Kumar R, Sharma N, Rolta R, Lal UR, Sourirajan A, Dev K, Kumar V (2020) *Thalictrum foliolosum* DC: An unexplored medicinal herb from north western Himalayas with potential against fungal pathogens and scavenger of reactive oxygen species. Biocatal Agric Biotechnol 26:01621. https://doi.org/10.1016/j.bcab.2020.101621
25. Lakshmanan G, Sathiyaseelan A, Kalaichelvan PT, Murugesan K (2018) Plant-mediated synthesis of silver nanoparticles using fruit extract of *Cleome viscosa* L.: assessment of their antibacterial and anticancer activity. Karbala Int J Mod Sci 4(1):61-68. https://doi.org/10.1016/j.kijoms.2017.10.007
26. Li Z, Liu R, Tang C, Wang Z, Chen X, Jiang Y, Wang C, Yuan Y, Wang W, Wang D, Chen S (2019) Cobalt Nanoparticles and Atomic Sites in Nitrogen-Doped Carbon Frameworks for Highly Sensitive Sensing of Hydrogen Peroxide. Small 16(15):1902860. https://doi.org/10.1002/smll.201902860
27. Lu Q, Eid K, Li W, Abdullah AM, Xu G, Varma RS (2021) Engineering Graphitic Carbon Nitride (g-C3N4) for Catalytic Reduction of CO2 to Fuels and Chemicals: Strategy and Mechanism. Green Chem 23;5394–28. https://doi.org/10.1039/D1GC01303C
28. Mohsen E, El-Borady OM, Mohamed MB, Fahim IS (2020) Synthesis and characterization of ciprofloxacin loaded silver nanoparticles and investigation of their antibacterial effect. J. Radiat. Res Appl Sci 13(1):416-25. https://doi.org/10.1080/16878507.2020.1748941
29. Moulton MC, Braydich-Stolle LK, Nadagouda MN, Kunzelman S, Hussain SM, Varma RS (2010) Synthesis, characterization and biocompatibility of “green” synthesized silver nanoparticles using tea polyphenols. Nanoscale 2(5):763-70. https://doi.org/10.1039/C0NR00046A
30. Nasrollahzadeh M, Shafiei N, Nezafat Z, Sadat Soheili Bidgoli N, Soleimani F, Varma RS (2020) Valorisation of Fruits, their Juices and Residues into Valuable (Nano) materials for Applications in Chemical Catalysis and Environment. Chem Rec 20(11):1338-93. https://doi.org/10.1002/tcr.202000078
31. Ndikau M, Noah NM, Andala DM, Masika E (2017) Green synthesis and characterization of silver nanoparticles using *Citrullus lanatus* fruit rind extract. Int J Environ Anal Chem 8108504. https://doi.org/10.1155/2017/8108504
32. Neal CJ, Gupta A, Barkam S, Saraf S, Das S, Cho HJ, Seal S (2017) Picomolar detection of hydrogen peroxide using enzyme-free inorganic nanoparticle-based sensor. Sci Rep 7(1):1-10. https://doi.org/10.1038/s41598-017-01356-5
33. Pariona N, Mtz-Enriquez AI, Sánchez-Rangel D, Carrión G, Paraguay-Delgado F, Rosas-Saito G (2019) Green-synthesized copper nanoparticles as a potential antifungal against plant pathogens. RSC Adv 9(33):18835-43. https://doi.org/10.1039/C9RA03110C
34. Pattanayak S, Mollick MMR, Maity D, Chakraborty S, Dash SK, Chattopadhyay S, Roy S, Chattopadhyay D, Chakraborty M (2017) *Butea monosperma* bark extract mediated green synthesis of silver nanoparticles: characterization and biomedical applications. J Saudi Chem Soc 21(6):673-684. https://doi.org/10.1016/j.jscs.2015.11.004
35. Polshettiwar V, Baruwati B, Varma RS (2009) Self-assembly of metal oxides into three-dimensional nanostructures: synthesis and application in catalysis. ACS Nano 3(3):728-36.

https://doi.org/10.1021/nn800903p

36. Priya RS, Geetha D, Ramesh PS (2016) Antioxidant activity of chemically synthesized AgNPs and biosynthesized *Pongamia pinnata* leaf extract mediated AgNPs–A comparative study. Ecotoxicol Environ Saf 134:308-18. https://doi.org/10.1016/j.ecoenv.2015.07.037
37. Rani S, Sharma B, Malhotra R, Kumar S, Varma RS, Dilbaghi N (2020) Sn-MOF@CNT nanocomposite: An efficient electrochemical sensor for detection of hydrogen peroxide. Environ Res 191:110005. https://doi.org/10.1016/j.envres.2020.110005
38. Ringmichon CL, Gopalkrishnan B, Dixit AP, Shimpi SN (2013) Pharmacognostical Evaluation of "Naga guining" Rhizome. IJPPR 5(1):4-8. https://www.researchgate.net/publication/296138438
39. Salari S, Bahabadi SE, Samzadeh-Kermani A, Yosefzaei F (2019) In-vitro Evaluation of Antioxidant and Antibacterial Potential of Green Synthesized Silver Nanoparticles Using *Prosopis farcta* Fruit Extract. Iran J Pharm Res 18(1):430. https://www.ncbi.nlm.nih.gov/labs/pmc/articles/PMC6487442/
40. Saratale RG, Saratale GD, Ghodake G, Cho SK, Kadam A, Kumar G, Jeon BH, Pant D, Bhatnagar A, Shin HS (2019) Wheat straw extracted lignin in silver nanoparticles synthesis: Expanding its prophecy towards antineoplastic potency and hydrogen peroxide sensing ability. Int J Biol Macromol 128:391-400. https://doi.org/10.1016/j.ijbiomac.2019.01.120
41. Saxena J, Sharma PK, Sharma MM, Singh A (2016) Process optimization for green synthesis of silver nanoparticles by *Sclerotinia sclerotiorum* MTCC 8785 and evaluation of its antibacterial properties. Springer Plus 5(1):1-10. https://doi.org/10.1186/s40064-016-2558-x
42. Schröfel A, Kratošová G, Šafařík I, Šafaříková M, Raška I, Shor LM (2014) Applications of biosynthesized metallic nanoparticles–a review. Acta Biomate (10)10:4023-4042. https://doi.org/10.1016/j.actbio.2014.05.022
43. Scorzoni L, de Paula e Silva AC, Marcos CM, Assato PA, de Melo WC, de Oliveira HC, Costa-Orlandi CB, Mendes-Giannini MJ, Fusco-Almeida AM (2017) Antifungal therapy: new advances in the understanding and treatment of mycosis. Front Microbiol 8:36. https://doi.org/10.3389/fmicb.2017.00036
44. Sharma RK, Yadav S, Dutta S, Kale HB, Warkad IR, Zbořil R, Varma RS, Gawande MB (2021) Silver Nanomaterials: Synthesis and (Electro/Photo) Catalytic Applications. Chem Soc Rev 50:11293-80 https://doi.org/10.1039/D0CS00912A
45. Shi X, Siahrostami S, Li GL, Zhang Y, Chakthranont P, Studt F, Jaramillo TF, Zheng X, Nørskov JK (2017) Understanding activity trends in electrochemical water oxidation to form hydrogen peroxide. Nature Commun 8(1):1-6. https://doi.org/10.1038/s41467-017-00585-6
46. Silva RA, Montes RH, Richter EM, Munoz RA (2012) Rapid and selective determination of hydrogen peroxide residues in milk by batch injection analysis with amperometric detection. Food Chem 133(1):200-04. https://doi.org/10.1016/j.foodchem.2012.01.003
47. Singh B, Gawande MB, Kute AD, Varma RS, Fornasiero P, McNeice P, Jagadeesh RV, Beller M, Zbořil R (2021) Single-atom (iron-based) catalysts: synthesis and applications. Chem Rev 121:13620-13697

https://doi.org/10.1021/acs.chemrev.1c00158

48. Singh N, Nambiar D, Kale RK, Singh RP (2013) Usnic acid inhibits growth and induces cell cycle arrest and apoptosis in human lung carcinoma A549 cells. Nutr Cancer 65:36-43. https://doi.org/10.1080/01635581.2013.785007
49. Sun N, Han Y (2019) Cytotoxic isoquinoline alkaloids from the roots of *Thalictrum foliolosum*. J Asian Nat Prod Res 23(1):1-8. https://doi.org/10.1080/10286020.2019.1694515
50. Tagad CK, Kim HU, Aiyer RC, More P, Kim T, Moh SH (2013) A sensitive hydrogen peroxide optical sensor based on polysaccharide stabilized silver nanoparticles. RSC Adv 3(45):22940-22943. https://doi.org/10.1039/C3RA44547J
51. Vanaja M, Gnanajobitha G, Paulkumar K, Rajeshkumar S, Malarkodi C, Annadurai G (2013) Phytosynthesis of silver nanoparticles by *Cissus quadrangularis*: influence of physicochemical factors. J Nanostruct Chem 3(1):1-8. https://doi.org/10.1186/2193-8865-3-17
52. Varma RS (2019) Biomass-derived renewable carbonaceous materials for sustainable chemical and environmental applications. ACS Sustainable Chem Eng 7(7):6458-70. https://doi.org/10.1021/acssuschemeng.8b06550
53. Vorobyova V, Vasyliev G, Skiba M (2020) Eco-friendly “green” synthesis of silver nanoparticles with the black currant pomace extract and its antibacterial, electrochemical, and antioxidant activity. Appl. Nanosci 10(12):4523-34. https://doi.org/10.1007/s13204-020-01369-z
54. Zare EN, Padil VV, Mokhtari B, Venkateshaiah A, Wacławek S, Černík M, Tay FR, Varma RS, Makvandi P (2020) Advances in biogenically synthesized shaped metal-and carbon-based nanoarchitectures and their medicinal applications. Adv Colloid Interface Sci 283:102236. https://doi.org/10.1016/j.cis.2020.102236

Figures

Figure 1

Plant of *Thalictrum foliolosum* DC.

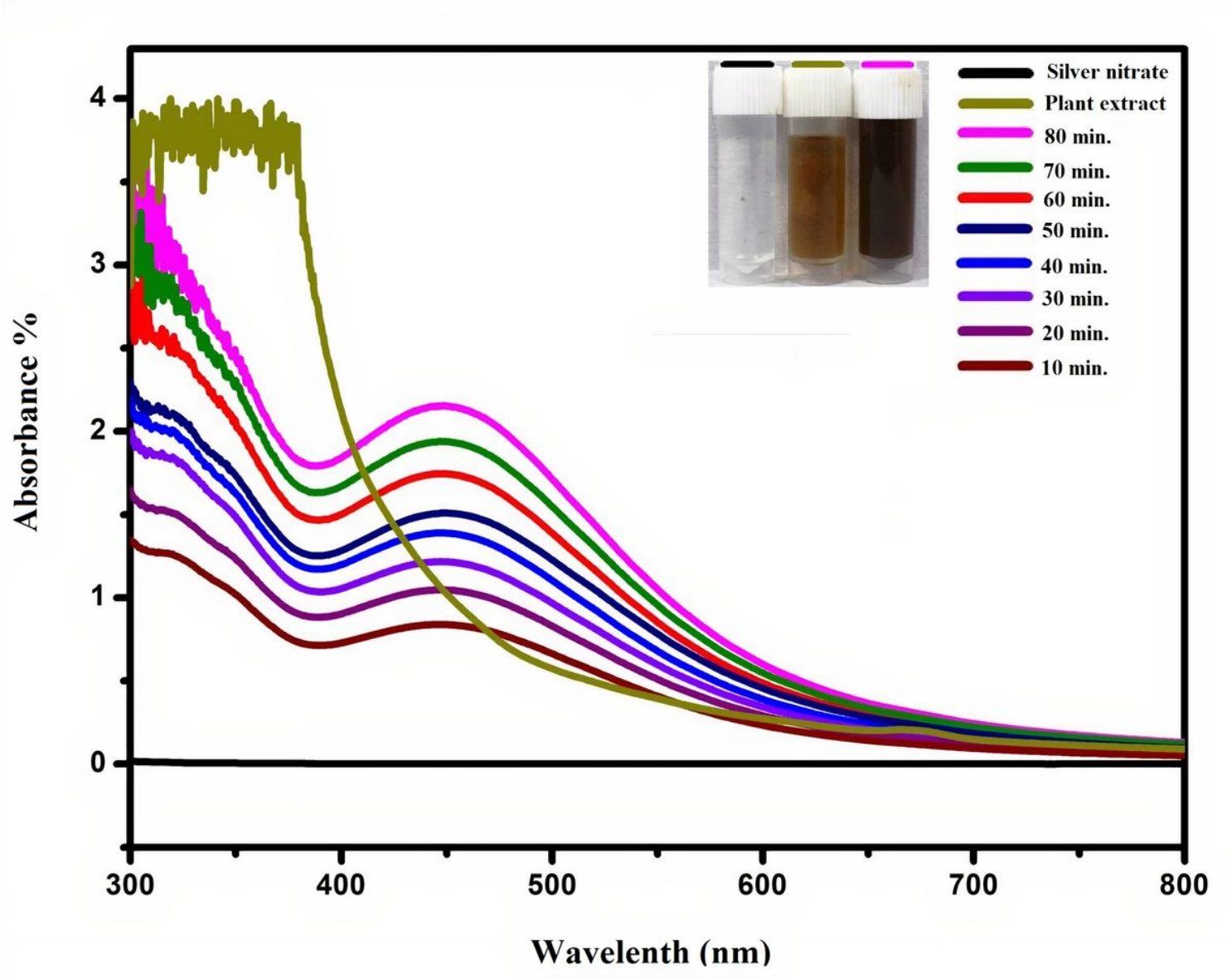

Figure 2

UV-visible spectra of TFLE, $AgNO_3$, and TF@AgNPs after (10-80 min.)

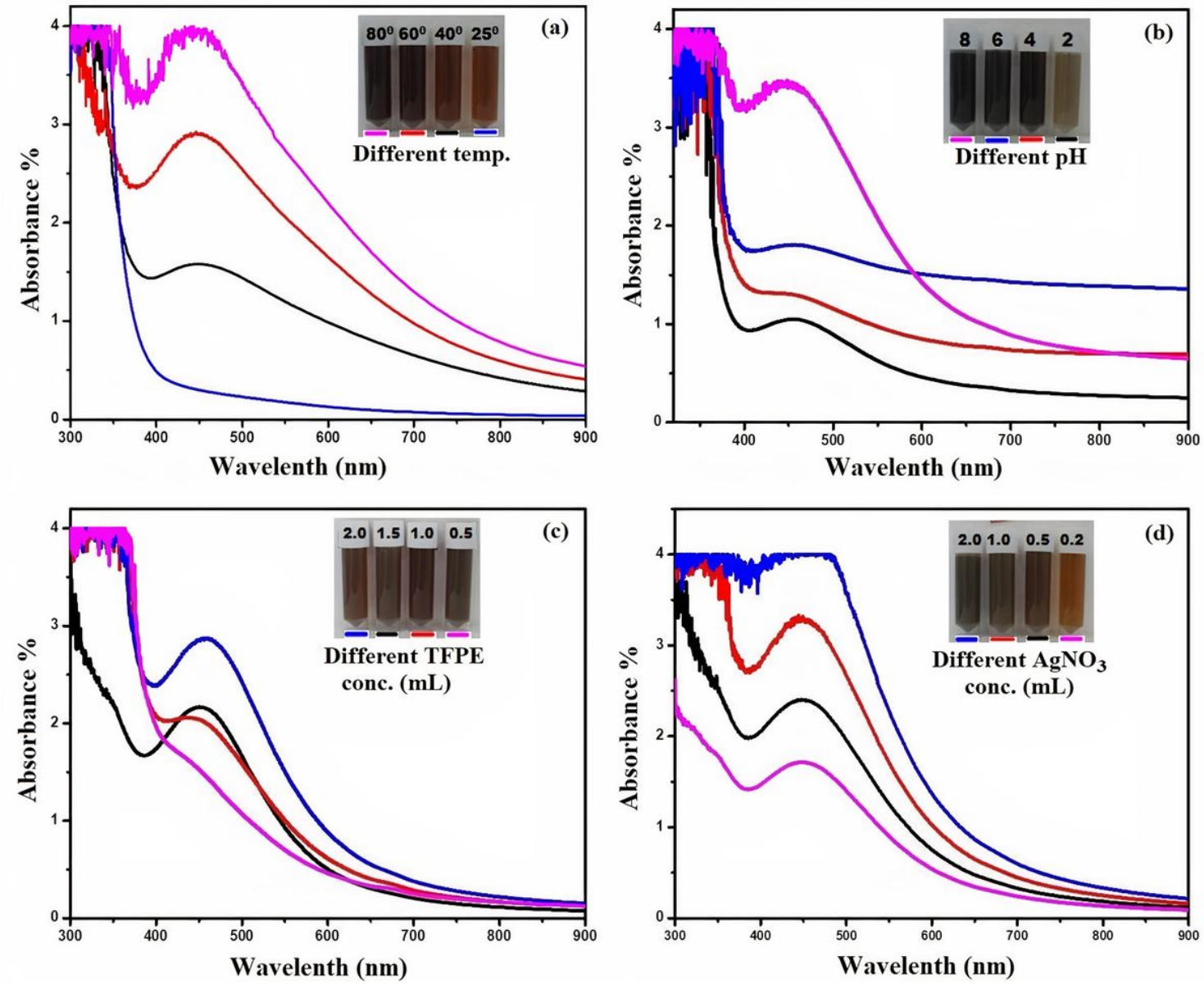

Figure 3

UV-Vis spectral analysis of bioengineered TF@AgNPs: (a) on different temperatures; (b) on different pH; (c) on different concentrations of TFLE; (d) on different concentrations of $AgNO_3$ solutions.

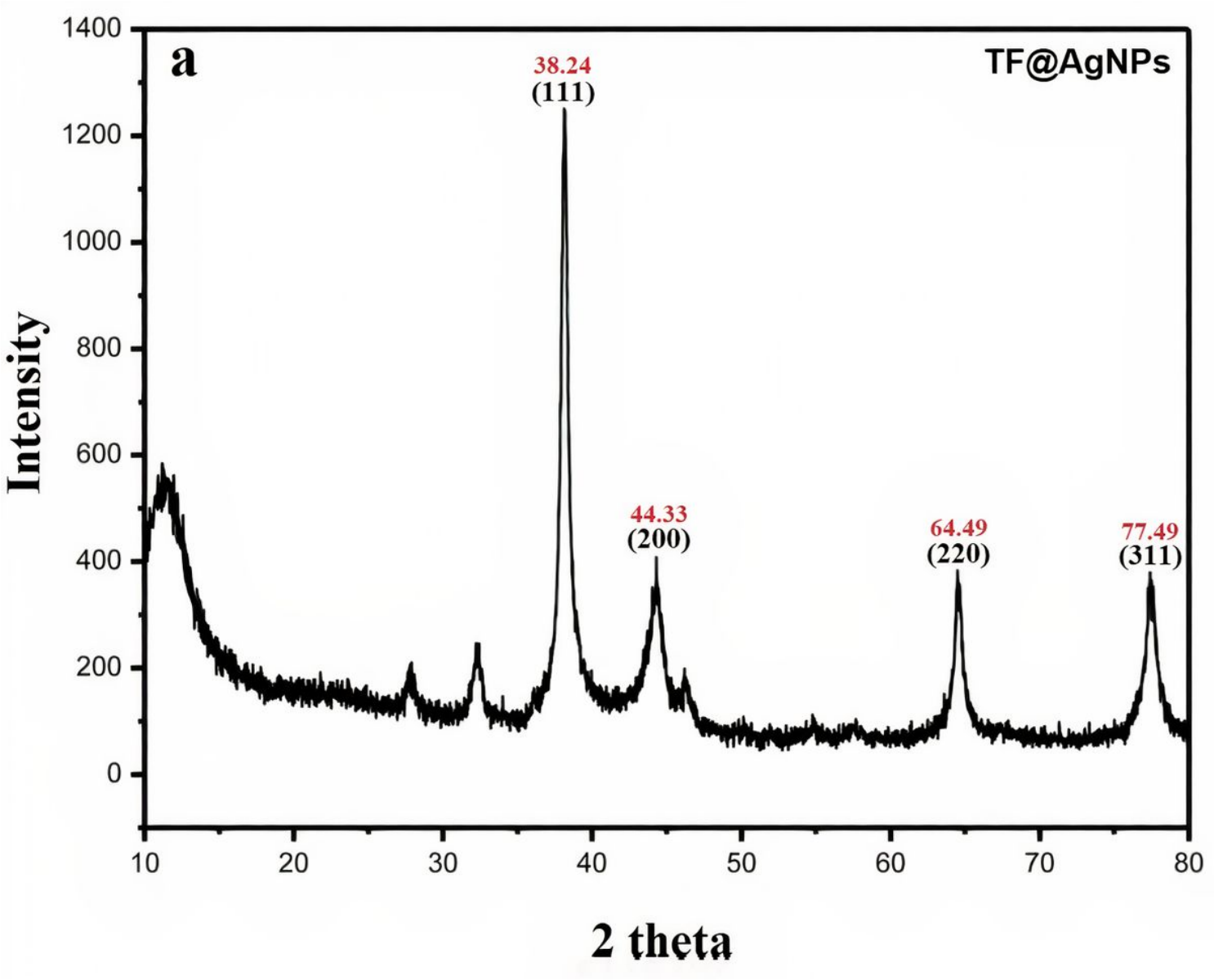

Figure 4

XRD spectra of bioengineered TF@AgNPs

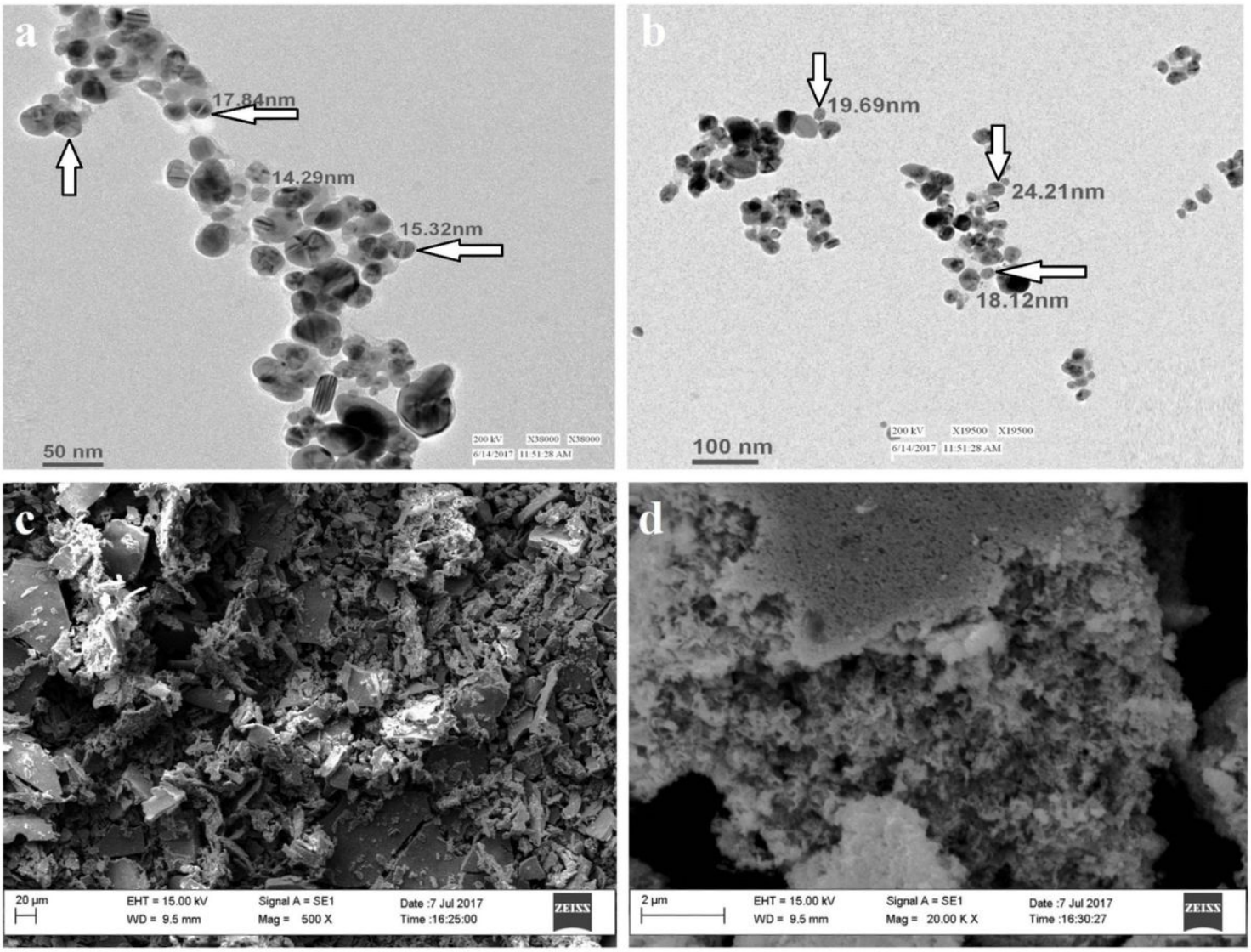

Figure 5

TEM images (a-b) and SEM images of TF@AgNPs (c-d).

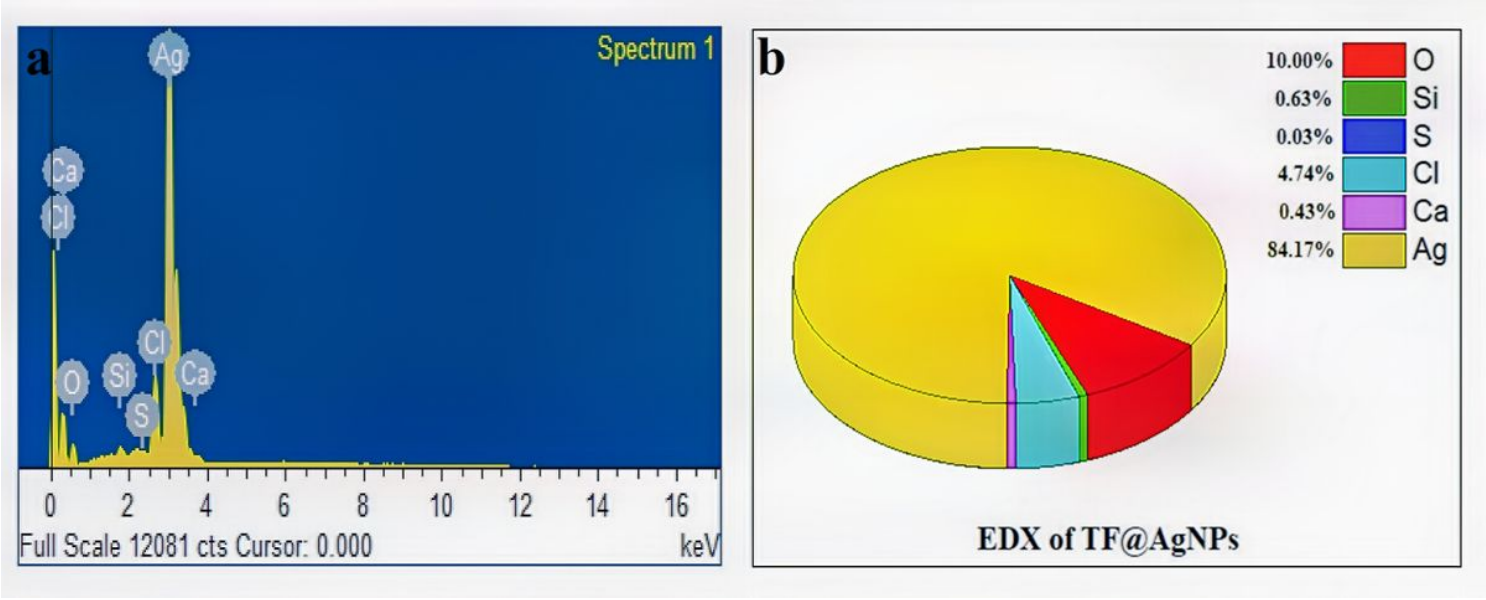

Figure 6

EDX analysis of TF@AgNPs (a) and elements percentage present in TF@AgNPs.

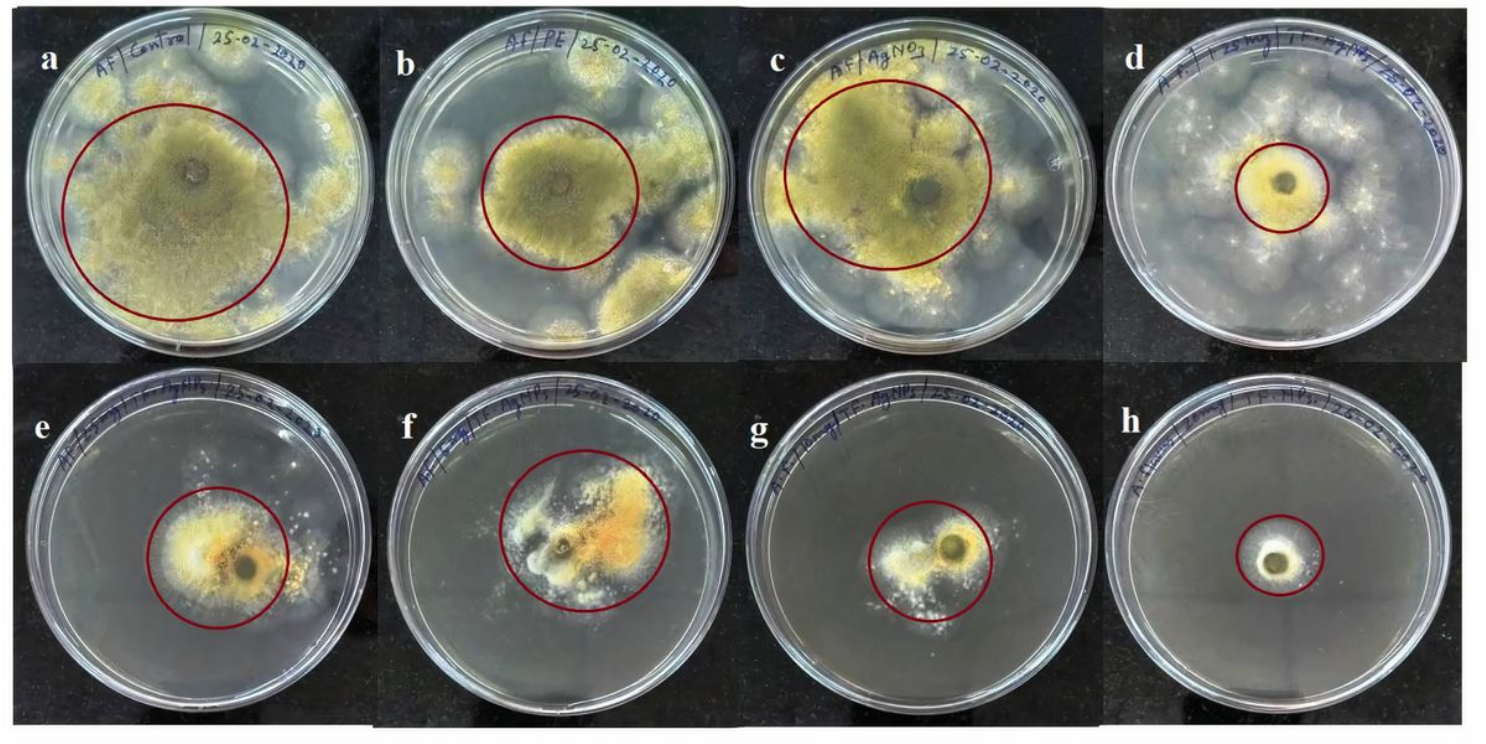

Figure 7

Antifungal activity of TF@AgNPs against: *A. flavus*. The rows represent (a) 0 (controls), (b) TFLE (c) $AgNO_3$, and different concentrations of TF@AgNPs: (d) 1.25, (e) 2.5, (f) 5, (g) 10, and (h) 20 mg / 20 mL in PDA.

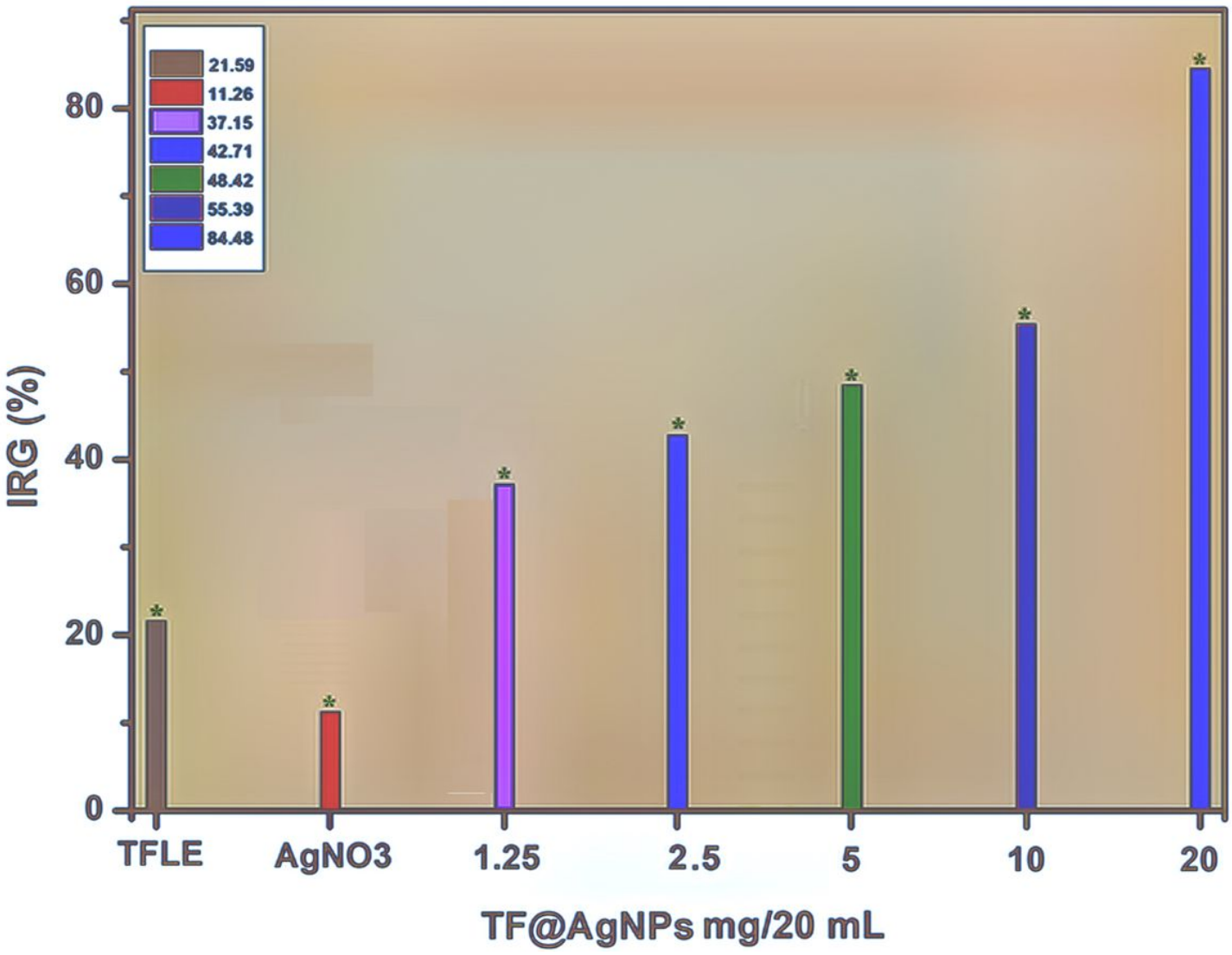

Figure 8

IRG (%) of TF@AgNPs against *A. flavus*. (*) indicates significant differences ($P < 0.05$) in comparison to their controls.

Figure 9

UV-Vis spectral analysis of TF@AgNPs and H_2O_2 at a different time spell, [Inset: vials i, ii, and iii represent TF@AgNPs, H_2O_2 and TF@AgNPs, and after 21 min reacting solution respectively].

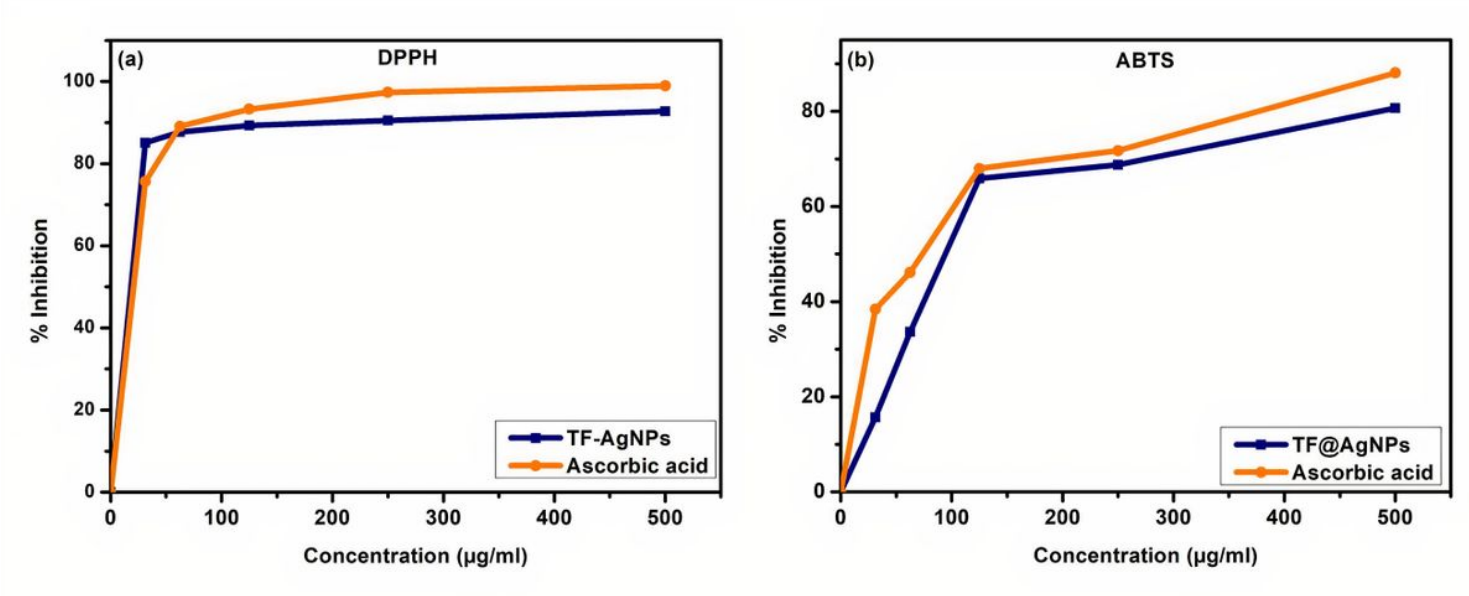

Figure 10

Free radical scavenging activity of TF@AgNPs, DPPH (a), ABTS (b).

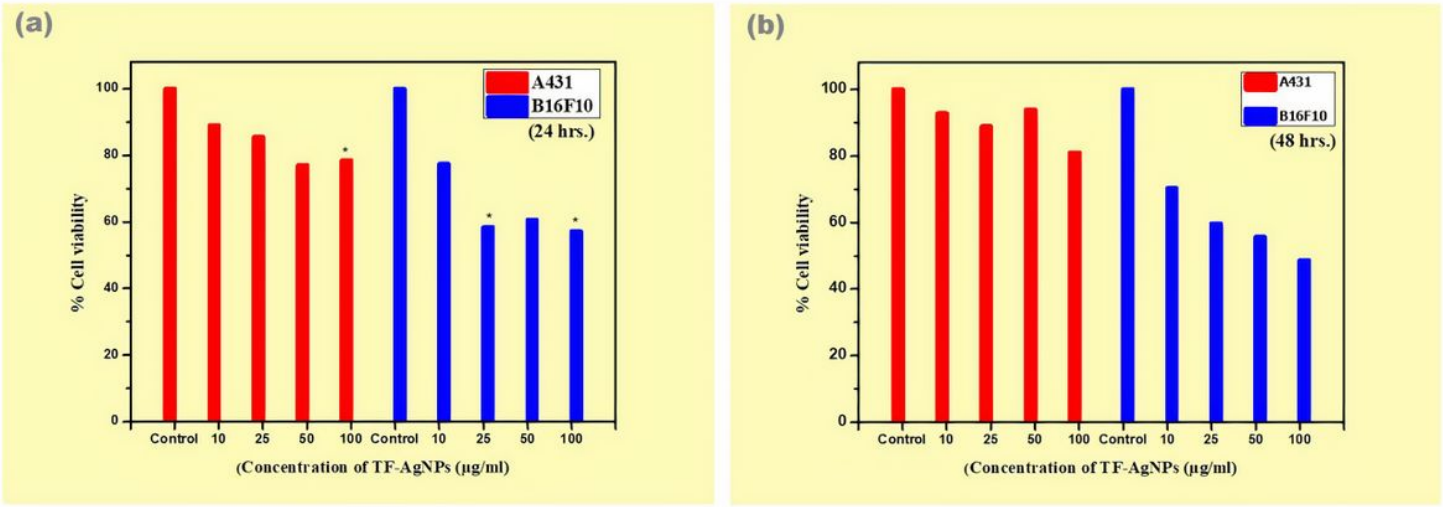

Figure 11

Melanoma cell line (B16F10) and Squamous carcinoma cell line (A431) viability percentages after incubation at different times (24 and 48 h) with varying concentrations of TF@AgNPs synthesized from THLE.

Supplementary Files

This is a list of supplementary files associated with this preprint. Click to download.

- GA.jpg

- Supplementaryfile.docx